Universidade de Lisboa

Faculdade de Farmácia

Langmuir-Blodgett films as a model of the skin barrier lipids – corneocyte interface

Bárbara Inês Lobo Belchiorinho Bernardino

Trabalho de Campo orientado pela Professora Doutora Petra Pullmannová, Categoria Professora Auxiliar, Farmaceutiká Fakulta – Univerzita Karlova, e coorientado pela Professora Doutora Liana Casquinha Silva, Categoria Professora Auxiliar, da Faculdade de Farmácia da Universidade de Lisboa

Mestrado Integrado em Ciências Farmacêuticas

2022

Universidade de Lisboa

Faculdade de Farmácia

Langmuir-Blodgett films as a model of the skin barrier lipids – corneocyte interface

Bárbara Inês Lobo Belchiorinho Bernardino

Trabalho Final de Mestrado Integrado em Ciências Farmacêuticas apresentado à Universidade de Lisboa através da Faculdade de Farmácia

Trabalho de Campo orientado pela Professora Doutora Petra Pullmannová, Categoria Professora Auxiliar, Farmaceutiká Fakulta – Univerzita Karlova, e coorientado pela Professora Doutora Liana Casquinha Silva, Categoria Professora Auxiliar, da Faculdade de Farmácia da Universidade de Lisboa

2022

This research project was developed under the Erasmus+ Programme in the Faculty of Pharmacy of Charles University (Farmaceutiká Fakulta – Univerzita Karlova) in Hradec Králové, Czech Republic, under the guidance of Doctor Petra Pullmannová.

FARMACEUTICKÁ FAKULTA
V HRADCI KRÁLOVÉ
Univerzita Karlova

Abstract

The skin protects the body against external influences from the environment and prevents excessive water loss. This effective barrier function is provided by the epidermal outermost layer, the stratum corneum (SC). It consists of approximately 10 to 25 layers of flattened dead cells, the corneocytes, surrounded by a lipid matrix, which is necessary for the proper function of the skin lipid barrier (SLB). These highly specialised lipids are mainly ceramides, free fatty acids and cholesterol, present at a 1:1:1 molar ratio. The composition and structure of skin lipids are closely related to epidermal homeostasis because changes in it disturb the correct performance of the lipid barrier, and may be the origin of some pathological conditions such as atopic dermatitis (AD). The goal of this study was to evaluate the behaviour of the skin lipid models at the air-water interface, mimicking pathophysiological conditions. We studied the impact of ceramide (Cer) and phytoceramide (PhytoCer) on the barrier properties and membrane structure of the SC lipid model composed of ternary or quaternary mixtures with free fatty acids (FFA (16-24)) and cholesterol (Chol). To investigate their behaviour, lipid monolayers were prepared using the Langmuir-Blodgett (LB) technique and the respective Surface Pressure (SP) - Mean Molecular Area (MMA) isotherms were measured. Lipid monolayers were transferred to a substrate and Atomic Force Microscopy (AFM) was used to analyse the structure of the monolayers as a function of their composition. At the same SP, higher MMA were observed for Cer-containing models, compared to analogous mixtures containing PhytoCer. These results show that in the PhytoCer-based model compression was achieved at lower SP, suggesting that the lipid molecules are more compacted than those in the Cer mixtures. Finally, AFM showed that the lipids present in the skin models were separated into different domains on the substrate. Inspecting the height differences and shapes, we determined two different domain types in Cer-based models and four different domain types in PhytoCer-based models.

Keywords: Stratum Corneum; Lipid Barrier; Ceramide; Monolayer; Langmuir-Blodgett

Resumo

A pele protege o organismo contra influências externas do meio ambiente e previne a perda excessiva de água. Esta eficaz função de barreira é proporcionada pela camada mais periférica da epiderme, o estrato córneo (SC). O mesmo é constituído por, aproximadamente, 10 a 25 camadas de células mortas achatadas, os corneócitos, rodeados por uma matriz lipídica, fundamental para o correto funcionamento da barreira lipídica da pele (SLB). Estes lípidos, altamente especializados, são maioritariamente ceramidas, ácidos gordos livres e colesterol, presentes, sensivelmente, na razão molar 1:1:1. A composição e estrutura dos lípidos da pele encontra-se fortemente relacionada com a homeostasia epidérmica uma vez que, alterações na mesma, perturbam o normal funcionamento da barreira lipídica, podendo estar na origem de algumas condições patológicas como a dermatite atópica (AD). O objetivo deste estudo foi avaliar o comportamento dos modelos lipídicos da pele na interface ar-água, mimetizando as condições patofisiológicas. Foi estudado o impacto da ceramida (Cer) e da phytoceramida (PhytoCer) nas propriedades de barreira e estrutura da membrana do modelo lipídico do SC composto por misturas ternárias ou quaternárias com ácidos gordos livres (FFA (16-24)) e colesterol (Chol). Para investigar o seu comportamento, foram preparadas monocamadas lipídicas através da técnica Langmuir-Blodgett (LB) e medidas as respetivas isotérmicas Pressão Superficial (SP)-Área Molecular Média (MMA). As monocamadas lipídicas foram transferidas para um substrato e utilizou-se a Microscopia de Força Atómica (AFM) para analisar a estrutura das monocomadas em função da sua composição. À mesma SP, foram observadas MMA mais elevadas nos modelos contendo Cer, em comparação com misturas análogas contendo PhytoCer. Estes resultados mostram que, no modelo baseado em PhytoCer, a compressão foi conseguida a SP mais baixas, sugerindo que as moléculas lipídicas estão mais compactadas do que as das misturas de Cer. Finalmente, AFM mostrou que os lípidos presentes nos modelos de pele foram separados em diferentes domínios no substrato. Investigando as diferenças de altura e formas, identificámos dois tipos diferentes de domínios no modelo contendo Cer e quatro no modelo baseado em PhytoCer.

Palavras-chave: Estrato Córneo; Barreira Lípídica; Ceramida; Monocamada; Langmuir-Blodgett

Ackonowledgements

I would first like to thank my thesis supervisors, Doctor Liana Silva and Doctor Petra Pullmannová for their availability, for all that they have taught me, their wise feedback, but also for all the effort invested and the trust they have placed in me. Without your guidance, this work would not have been successfully completed.

I want to acknowledge my parents, brother and grandparents who followed every step of this journey, always supported me in every decision and encouraged me to follow my dreams. Thank you very much for everything you do for me every day.

Ana Marta, Adriana and Catarina, who crossed my path on the first day of this adventure and accompanied me through all the difficulties on this journey, I am very thankful to you! We began and finished together, I will never forget the moments we spent during these five years.

I also want to thank my boyfriend, André, for always being there for me, in good and bad moments, with the right words and the comfort I need. I am grateful for who you are and I am so lucky to have you in my life!

Last but not least I want to express my gratitude to all my family and friends for all their support and all those who came into my life and made a difference in my path.

Thank you!

Abbreviations

AD	Atopic Dermatitis
AFM	Atomic force microscopy
Cer	C24 Cer [NS]; N-lignoceroyl-D-erythro-sphingosine
Chol	Cholesterol
CholS	Cholesterol sulfate
FFA	Free Fatty Acids
LB	Langmuir-Blodgett
LIG	Lignoceric acid
PhytoCer	C24 Cer[AP]; α-hydroxy-N- lignoceroylphytosphingosine
PhytoSO	Phytosphingosine
SC	Stratum Corneum
SD	Standard Deviation
SL	Sphingolipids
SLB	Skin Lipid Barrier
SO	Sphingosine
SP	Surface Pressure

Index:

Figure Index:

Table Index:

1 Introduction

1.1 Skin

The skin is composed of the epidermis, the dermis, (1) which makes up most of the skin and contains mainly fibroblasts embedded in an acellular collagen/elastin matrix that makes up most of the skin, (2) and the subcutaneous fat tissue. The epidermis is the outermost layer of the skin and consists of four distinctive layers. Each layer displays one of the sequential differentiation stages of the major cell type in the epidermis keratinocytes. The layers are the superficial stratum corneum (SC), stratum granulosum, stratum spinosum, and the inner most stratum basale. (1)

Despite the extensive research done in this area, little is known about the fundamental structure–permeability relationships of membranes containing ceramides and the lipid composition of diseased skin. This is the main impediment to the rational design of skin barrier repair agents or to a wider application of transdermal drug delivery. (3)

1.1.1 Function

The primary function of the skin is to protect the body from water loss and entrance of potential toxic compounds, allergens, irritants and microbes. (4)

The skin barrier is localised in SC, which contains the cornified cells – corneocytes – in the terminal stage of differentiation, and extracellular lipids. The extracellular lipid domains between the corneocytes (2) are the primary barrier to the permeation of xenobiotics across the skin. (Figure 1) (5)

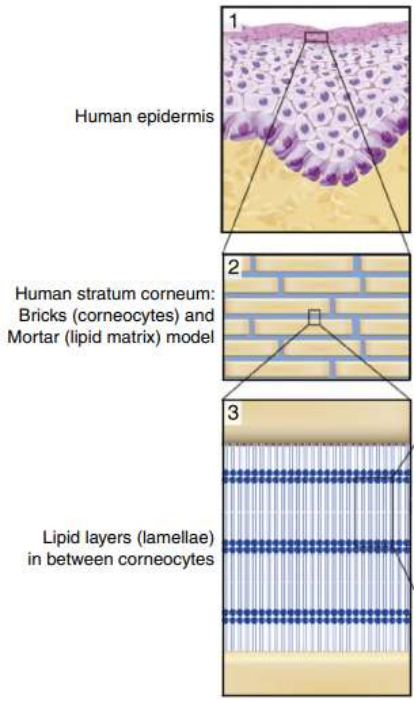

Figure 1: Lipid organization in human epidermis, specifically in the SC. Adapted from (1). SC, the outermost layer of the epidermis, is formed up of dead cells (corneocytes) embedded in a lipid matrix, also known as the "brick and mortar" structure. The intercellular lipids are organized in layers (lamellae).

1.1.2 Structure of Stratum Corneum

Human SC is a transparent thin layer that ranges in thickness from 10 to 20 µm (1) and is made up of 10 to 25 corneocyte layers that are roughly parallel to the skin's surface. (6) Corneocytes are terminally differentiated, keratin-filled, elongated, enucleated and flat-tened. (7) They are embedded in the extracellular lipid regions – lipid matrix. (2) The corneocytes are covered by a layer of densely cross-linked proteins, the cornified envelope. (5)

1.1.2.1 Corneocyte Lipid Envelope

The first lipid layer of the multilamellar skin barrier membranes is covalently anchored to the corneocyte surface and forms the corneocyte lipid envelope (CLE). (8)

CLE is meant to serve as a template for the orientation of the free barrier lipids and prevent permeable boundaries between the lipids and cells, is likely to help the transition from fluid to crystalline lipids as well. (9)

Forslind proposed a model for lipid barrier organisation named domain mosaic model. According to him, the SC's lipids are found in large ordered domains (crystalline or gel

phases) that are bordered by areas of liquid, crystalline lipids. (7) This "mortar" made of lipids is thought to be the primary route for the diffusion of substances into the body. (2) It is composed of a nearly equimolar mixture of ceramides, cholesterol (Chol) and free fatty acids (FFA). There are also trace amounts of cholesterol sulfate (CholS). (8) This ratio is critical for normal organization into the lamellar membrane structures that are primarily in charge of maintaining the homeostasis of the epidermal barrier. (2)

The majority of the lipids in the lipid lamellae are packed laterally in an orthorhombic manner (very tight packing). (5) Nevertheless, it also forms hexagonal lateral packing, which has more rotational freedom. (Figure 2) (6) The conformational ordered orthorhombic phases with the highest packing densities control transdermal fluxes; the more of these phases there are, the more effective the SC's barrier is. (10)

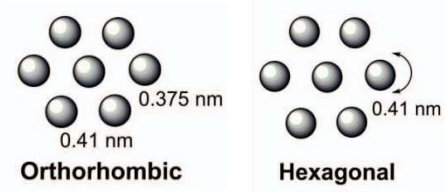

Figure 2: Lateral packing of the SC lipid membranes. Adapted from (7). Possible arrangements of the lipids: a very dense, ordered orthorhombic organization and a less dense, ordered hexagonal organization.

The acidic environment relative to the pH of the majority of human tissues is necessary for the protective barriers of human skin to function properly. This environment is able to ward off potentially dangerous microbes, activate enzymes that produce biochemically unusual skin lipid barrier (SLB), inhibit serine proteases that would impede SC integrity and/or cohesion, and stop the release of proinflammatory cytokines. (11)

1.2 Skin Lipids

Mammalian bodies´essential barrier function is carried out by skin lipids. (12) They are produced by keratinocytes, which are found in the epidermis, and are then transformed to their more polar precursors, which are then stored in lamellar bodies using catabolic enzymes. (6) The combined lipid and protein contents of these lamellar bodies are secreted into the intercellular space after their fusion with the stratum granulosum at the apical plasma membrane. (2) The final "processing" step that enables efficient

permeability barrier development in the SC is the following hydrolysis of these lipid precursors. (2)

1.2.1 Ceramides

Ceramides make up about a third of all lipid molecules, or a half of all lipids by weight and have been shown to induce a plethora of cellular functions. (6) They are the main metabolite in the metabolism of sphingolipids (SL) and a crucial intermediate in the production of glycosphingolipids and sphingomyelin, besides being involved in numerous cellular processes, including cell to cell recognition, intercellular adhesion, motility and differentiation. (13)

These lipids are vital components of CLE. (14)

Ceramides are composed of a sphingoid backbone, which is a long-chain amino alcohol, (6) connected to a fatty acid with a variable chain length and degree of saturation by an amide bond as showed in Figure 3A. (15)

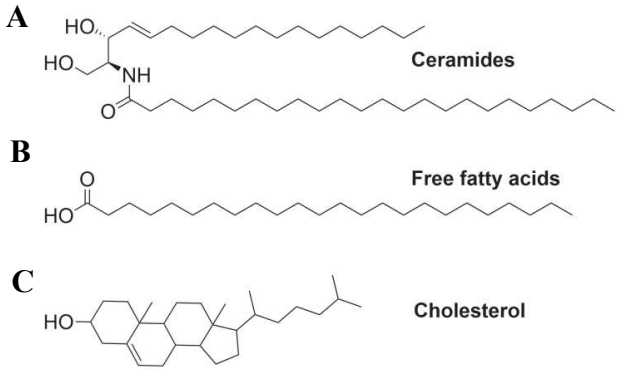

Figure 3: Molecular structure of SC lipids. Adapted from (7). (A) Ceramides are composed of a fatty acid chain linked to a SO base. (B) FFA are 14–34 carbons long, mostly saturated and unbranched. (C) Chol has a small head group made up of a -hydroxyl group at C3, a tetracyclic ring with an angular methyl group on one side, and an isooctyl chain attached to C17.

Ceramides structures and their aggregation mechanisms exhibit significant heterogeneity, which may confer resistance to the diverse external stressors that the skin barrier is constantly exposed to. (16)

In the human SC, 15 classes of ceramides have been found thus far. (6) As we can see in Figure 4, ceramides nomenclature according to Motta is based on the type of sphingoid base, which can be either sphingosine (SO), dihydrosphingosine (dS), phytosphingosine (PhytoSO), which is only present in a small number of human tissues,

and 6-hydroxysphingosine (H), which is unique to the epidermis. (5) Cer[NP] is typically the most prevalent subclass, and the acyl-ceramides subclasses ([EOdS], [EOS], [EOP], and [EOH]) account for 8–13% of all ceramides. (Figure 4) (1)

The fatty acyl chain of ceramides molecule can be saturated or monounsaturated, without further substitution (N), α-hydroxylated (A), or ω-hydroxylated (O) in the case of extremely long chains. (6) Long hydrocarbon chains and a few of polar hydroxy and amino groups give ceramides a very low polarity, a high degree of hydrophobicity, and a high melting point, which reduces their miscibility with other membrane lipids. (17)

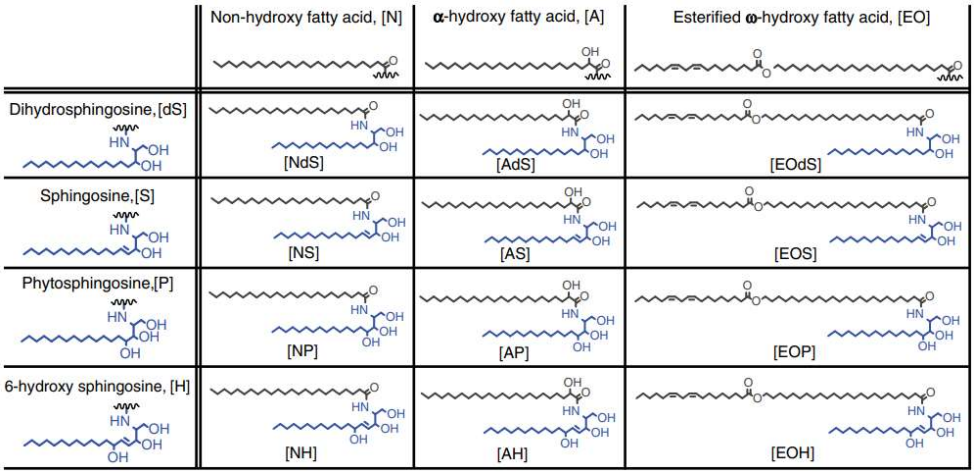

Figure 4: Chemical structures of the SC ceramides and their shortened nomenclature. Adapted from (1). A fatty acid chain connected to a SO base forms ceramides. Both chains show a variety in the length of their carbon chains and, as a result, ceramides' total carbon chain lengths differ widely. Additionally, ceramides may contain a further functional group, creating several subclasses.

The acyl chains that constitute the human skin barrier ceramides are very long (20–26 carbons) or ultra-long (28-32 carbons). (8) Each acyl chain length's abundance varies from tissue to tissue (18) and they each have a different biological function. (19) For instance, ceramides with very long chains have a stronger tendency to form tubular structures, (15) which probably originate to stabilize the membrane due to interdigitation of the long fatty acid chain into the other membrane leaflet. (18) Additionally, C24-SL, specifically C24-sphingomyelin, play a significant role in modulating the distribution of Chol on the plasma membrane. (18)

However, different lengths of the ceramide acyl chain has an impact on phase behaviour and packing in model SC. (19) According to studies performed with mixtures containing Cer[NS], shorter chains pack less effectively due to reduced hydrophobic

interactions, while having the same polar head shape and hydrogen bonding capacity as the natural long-chain Cer[NS]. (4) Furthermore, It is known that very long C24 Cer[NS], prefers an extended (splayed-chain) conformation where the fatty acid is joined with the very long ceramide chain. (16)

Studies show that membrane structure is altered and permeability diminished when C24 Cer[NS] is replaced by C16 Cer[NS]. In comparison to very long chain C24 Cer[NS]-based membranes, the long chain C16 Cer[NS]-based model membranes offered a less effective water barrier. While C24 Cer[NS] was well miscible with the investigated fatty acids, C16 Cer[NS] caused the formation of lamellae with a shorter repeat distance and was less miscible with fatty acids. (8) This was caused by a reduced percentage of tightly packed orthorhombic domains that are continuously enriched in long ceramides, as well as phase separation and shorter lamellar periodicity compared to native very long ceramides. The main reason for this outcome is that, unlike their shorter equivalents, only the very long ceramides mixes well with the long FFA. (3)

Depending on the level of hydration, ceramides exhibit a complex polymorphic phase behaviour and a propensity to form metastable phases. (20) As a result, until thermodynamic equilibrium is reached, the lipids will tend to deform the membrane and organize into structures that reduce membrane tension. (18) This means that ceramide-containing mixtures exhibit the coexistence of multiple phases, which are typically represented by intricate phase diagrams. (21)

Ceramides cause significant changes in the biophysical characteristics of membranes, such as the formation of highly ordered gel domains, an increase in the packing of the fluid phase, a change in membrane permeability, the induction of the lamellar-to-non-lamellar phase transition, and significant morphological changes. (18) Therefore, the balance between long chain versus very long chain, as well as saturated versus unsaturated ceramide species, may determine the overall biophysical effect of increasing ceramide levels. For example, saturated ceramides are known to segregate into highly ordered gel domains and to have a greater tendency to improve the order of fluid membranes. (15)

It is also described that ceramides might self-assemble into large channels, cylinder-shaped elements with regenerative mechanical characteristics that can transport proteins through membranes. (17)

Ceramides can significantly alter membrane properties when combined with other lipids. In fact, Chol influences ceramides miscibility in the membrane as the gel phase created by ceramides is destabilized by Chol. (20) There may be a delicate balance between these two lipids in biological membranes that controls the ordering state and the properties of the membrane. (21)

1.2.2 Free Fatty Acids

FFA are another lipid class found in the human SC. They are primarily saturated and unbranched as represented in Figure 3B. (5) The skin barrier's FFA range in length from 14 to 34 carbons, (6) of which the most common ones have 24 (Lignoceric Acid (LIG)) and 26 (Cerotic Acid) carbon atoms in their chain. (5) About 50% of the SC's fatty acids originate from these two species. (6) They are essential for the existence of such a orthorhombic lipid organization. (1)

1.2.3 Cholesterol

Chol is the primary sterol in the SLB and is crucial for the proper operation of the skin barrier, helping to ensure proper lamellar and lateral structure and lipid fluidity. (6) As shown in Figure 3C, the molecule contains a quite rigid planar tetracyclic ring with an angular methyl group on one side and an isooctyl chain attached to C17 as well as a small head group made up of a -hydroxyl group at C3. (22)

Because the skin barrier lipids are exceptionally structurally heterogeneous, largely unavailable commercially, have a complex polymorphism, and need high-temperature annealing in vitro, (11) the relationships between their structure-activity are poorly understood. (4)

Studies in artificial membrane systems, though significantly less complex than biological membranes, (17) actually offer a way to comprehend the interactions between ceramides and other lipid species, which have led to advancements in this field. (23) Research in this area will advance through close interaction between scientists from multiple fields as well as through technological advancements (such as mass spectrometry imaging and fluorescent probes), which allow for a better understanding of the composition, interactions, trafficking, and metabolism of membrane lipids. (24)

1.3 Diseases

Lipids do play a crucial structural role in cells, as well as serving as signalling molecules in a number of cellular processes, including the mobilization of stem cells, the regulation of receptor proteins, cell growth, senescence and vesicular trafficking. (17)

Ceramide is implicated in many cellular processes, but some of those that have been linked to human disease include apoptosis, proliferation, and survival. (25)

Numerous pathologies, such as cancer (26), cystic fibrosis (27), neurodegenerative illnesses (28), epilepsy (29), diabetes mellitus type 2 (30), cardiovascular pathologies (31) and wound healing (32) are linked to a variety of ceramide species.

Ceramides have a variety of biological and pathological effects. Structural properties of ceramides, specifically their high hydrophobicity and capacity to establish a strong network of H-bonds, are responsible for changes in permeability, fluidity and lateral organization of biological membranes, inducing the transition to nonlamellar phases. (17) Protein activity and distribution may be affected, and signalling pathways may be activated. (17) Furthermore, ceramide is able to change membrane permeability (33), to form tubule-like structures (18) and ceramide-enriched domains, necessary for the clustering of membrane receptors and ensuing activation of signalling pathways (34) that mediate a particular cellular event, such as protein and lipid sorting. (18) Ceramides may also act as second messengers, as several putative direct targets have been discovered, including protein kinase C, protein phosphatase A2, and cathepsin D. (34)

Increased ceramide levels improve the permeability of a variety of membrane systems to small molecules and proteins.(17)

Farber Disease is a pathology characterized by a build up of ceramides in the lysosomes. It is an autosomal recessive disease, caused by mutations that inhibit ceramides degradation. (35) Traditional symptoms are the development of subcutaneous nodules, stiffness and deformation of the joints, as well as the development of a hoarse voice due to laryngeal involvement, with potential complications at the cardiac, pulmonary, and central nervous systems. (36)

Additionally, a number of pathological conditions have been linked to the modulation of mitochondrial Chol content. (37) Their increased levels, for example, were reported in hepatocellular carcinoma in humans. (38)

Other SL have also been looked into as potential biomarkers to predict disease in the general population due to their critical role in maintaining homeostasis within the body. (17) According to studies, SO is essential for the host's defence against Pseudomonas aeruginosa and other lung infections. These molecules play a special role as tumour suppressors by preventing the proliferation of cancer cell lines and inducing apoptosis. (24) It is known that PhytoSO has therapeutic potential for the treatment of inflammatory and proliferative cutaneous diseases and that it can supplement current acne treatments by acting as an active cosmetic ingredient. (24)

An altered skin lipid profile is also present in many chronic skin diseases. (2)

Atopic Dermatitis (AD) is characterized by either a rise in transepidermal water loss or a fall in water-holding capacity. (39) Moreover, in non-lesional AD SC, a higher proportion of hexagonally organized lipids was found, which suggests a less dense lipid organization. (1) When compared to the normal skin sites of healthy people, the affected sites of AD patients had significantly lower levels of total ceramides, (39) including phytoceramides. (13) Thus, we can infer that the ceramides profile is a potential indicator of AD and a marker for its prognosis. (39) Recent studies also revealed that AD patients had higher proportions of C16 ceramides with "long" acyl chains (such as C16 Cer[NS]) and lower levels of SO-based C24 Ceramides with "very long" acyl chains (such as C24 Cer[NS]). (8) The increased ratio of long/very long ceramides is most likely caused by inadequate elongation of the fatty acids used by ceramide synthases. (19) This is supported by the fact that there are more shorter FFAs, particularly C16:0 and C18:0, and less very long chain FFAs (24 carbon atoms) than in healthy skin. (1) Additionally, non-lesional AD skin have a lower Cer/Chol ratio. (1)

Lamellar ichthyosis is a skin disease distinguished by the absence of the transglutaminase 1 enzyme, which is responsible for crosslinking of the cornified envelope. In addition, a sharp decline in the FFA level in the SC lipid matrix was associated with lower FFA/Chol and FFA/Ceramide ratios. A significant increase in lipids with a hexagonal packing was also seen, at the detriment of lipids with an orthorhombic packing. Distinct lipid transporters engaged in lipid production may be connected to the origin of a different SC lipid composition. (1)

A persistently inflamed skin condition called psoriasis is marked by aberrant epidermal proliferation that results in inadequate differentiation. This condition may possibly be

caused by mutations in the genes encoding for cornified envelope proteins. Studies reported a decline of Cer[NP] and Cer[AP] subclasses but a rise of Cer[NS] and a reduction in the ceramides chain length. The fact that lesion regions are where lipid changes are most noticeable suggests that mechanisms like inflammation or modifications to the differentiation process are responsible for the observed variations in SC lipid properties. (1)

Although topical application of skin-identical lipids or their analogues has a strong potential to restore the SLB in such diseases and reduce inflammation, (3) a greater comprehension of the physical chemistry of ceramides and the molecular configuration of the skin lipid membranes is required for more logical design of such therapies. (6)

1.4 Langmuir-Blodgett Technics

The Langmuir-Blodgett (LB) method is based on the unique ability of organic molecules such as lipids, phospholipids, or glycolipids to position themselves at an air/water interface between the gaseous and liquid phases in order to minimize their free energy and form an insoluble monolayer known as a Langmuir film. (40)

When compared to other model membrane systems, Langmuir monolayers have an advantage since it is simple to adjust variables such molecular packing, physical state, lateral pressure, and composition. (41)

A floating monolayer may deposit on a solid substrate if it passes through the solid surface. The process is called LB deposition. (42)

1.4.1 Surface Pressure

Delivering a measured volume of solution with a known concentration spreads the monolayer. By sliding the barrier along the trough edges after the volatile solvent has evaporated, the monolayer can be compressed or expanded. The area per molecule ($\hat{A}_M$) is determined by the geometrical area (A) of the surface that is occupied by a monolayer and the quantity of amphiphile on the surface (N_M) (Equation 1). This number can be used to calculate the average area each molecule occupies at specific locations during the compression of the film according to the equation (42):

$$\hat{A}_M = A / N_M \qquad (1)$$

Due to the attractive interactions of the water molecules at the interface, the surface tension can be thought of as a negative pressure. The presence of a monomolecular film on a liquid surface lowers the system's free energy by fostering interactions between the hydrophilic polar group and the water surface molecules, which lowers the surface tension. In the presence of surfactants, the resultant decrease in surface tension causes an expansion of the air/water interface. The amphiphile molecules begin to interact and have a repellent effect on one another, especially their hydrocarbon chains. (40) The force applied by the film per unit length is designated as SP (π) and is obtained by subtracting the surface tension of pure water (γ) with the surface tension of the film (γ0). (Equation 2) (42) This equality means that the maximum SP for a monolayer on water at 20˚C is 72.8 mN/m, although typical values are much lower. (40) By measuring the vertical pull of surface tension on a wet Wilhelmy plate hanging through the surface, the surface tension can be determined. An electrobalance or a delicate spring with a position sensor is used to measure the force. (43) The SP (π)-area (A) isotherm diagram is typically used to track the formation of a monolayer at the air/water interface. (40)

$$\Pi = \gamma - \gamma 0 \qquad (2)$$

1.4.2 Surface-active molecules and Monolayer Formation

Insoluble Monolayers are formed at the air-water interface by amphiphiles with a strong hydrophobic moiety (practically insoluble in water) and a hydrophilic moiety that can anchor molecules to the water surface. (42)

The balance between these two opposing forces, which is controlled by the size of the hydrophobic tailgroup (the length of the alkyl chain) and the potency of the hydrophilic headgroup (its size, its polarity, its charge and its hydration capacity), is what allows amphiphiles to form monolayers. (40)

One of two methods can be used to spread the amphiphile in order that it can form a monolayer on a water surface: When placed on a surface, drops or crystals of the amphiphile spread on their own to form a monolayer, until either the bulk material is used up or equilibrium is reached with the spread monolayer. The solvent on the surface should have a positive spreading coefficient and be insoluble in the subphase like hexane, benzene, and chloroform. (42)

Following the evaporation of the solvent, the interfacial film develops into a monomolecular layer, which is one molecule thick, with the headgroups immersed in

the water and the tailgroups keeping outside (in direction to the gas phase). This particular orientation is defined by the amphiphiles, known as surfactants for surface active since they are found at the air/water interface. (40)

1.4.3 Monolayer Deposition

The deposition of additional layers on the surface may result from the substrate passing through the monolayer more than once, forming multilayer films. (42)

The SP needs to be high enough for the monolayer to be in a condensed state for the deposition to be successful, and the film must always be condensed using an automated system that moves the barrier to maintain a constant surface pressure (SP) as the film is removed (Figure 5). Typically, a SP between 20 and 40 mN/m is employed. The transfer ratio (TR), which, at constant SP, is the ratio of the area decrease on the subphase surface to the area of substrate, is used to determine the efficiency of deposition. This value should be one. (42)

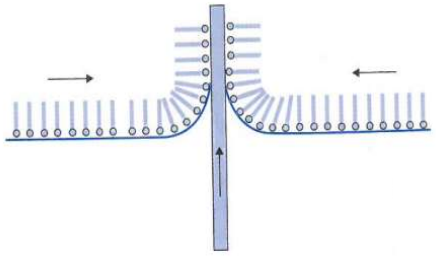

Figure 5: The LB deposition process. Adapted from (42). Solid ascending through a monolayer.

The monolayer is typically formed during emersion of a hydrophilic substrate when hydrophilic substrate and the hydrophilic headgroups come into contact with the surface. The monolayer will be transferred during immersion if the substrate surface is hydrophobic, reacting with the hydrophobic alkyl chains. The substrate may be immersed in the subphase prior to the formation of the monolayer for a hydrophilic surface. A hydrophilic substrate changes to hydrophobic after the transfer of the first monolayer, and a second monolayer is then deposited at the immersion. A hydrophilic substrate, on the other hand, changes from being hydrophobic, and the second monolayer is transferred during emersion. On each routing process of the surface, subsequent single layer depositions will accumulate to form multilayers. The most common configuration of a stack that results from this deposition mode, known as Y-type (Figure 6A), is head-to-head and tail-to-tail. Figure 6B shows an X-type deposition

when the floating monolayer only transfers during the substrate's immersion, and Figure 6C shows a Z-type deposition when it transfers during the substrate's emersion. (40)

The type of deposition is influenced by the subphase, amphiphile, SP, and number of layers deposited during the deposition process. (42)

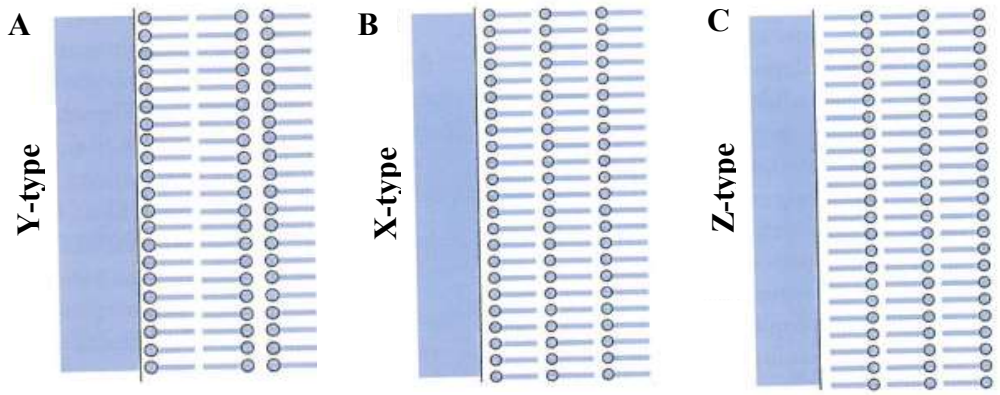

Figure 6: Structures for Y-type (A) LB deposition, X-type (B) LB deposition and Z-type (C) LB deposition. Adapted from (42). (A) A multilayer LB film with a hydrophilic substrate is most likely to have a Y-type deposition structure. (B) Other potential structures include the X-type LB deposition for oleophilic substrates and (C) the Z-type LB deposition in the case of hydrophilic substrates.

1.4.4 Monolayer Stability

One requirement for complex organized lipid LB films with high structural quality is the monolayer stability and, consequently, the monolayer homogeneity. (40)

Monolayer material will spontaneously spread to form a monolayer when it is placed on a water surface. Until the bulk material is exhausted or the monolayer and bulk material have reached equilibrium, this process continues. A monolayer will eventually experience an irreversible collapse if it is compressed further. (42)

Monolayer stability is primarily influenced by the monolayer's ability to dissolve into the subphase and by its mechanical resistance to overcompressions. The monolayer should not be compressed at SP's higher than the equilibrium spreading pressure in order to reach the equilibrium. The equilibrium spreading pressure is the pressure at which the monolayer, which is a two-dimensional state, and the crystal, three-dimensional state, are at equilibrium. The monolayer tends to aggregate into crystals through a nucleation and crystalline growth process at any SP higher than this. The solubility of the amphiphile monomers in the subphase has an impact on the monolayer's stability as well. It is crucial to keep in mind that a floating monomolecular

film is in a metastable state; as a result, if the monomolecular film is not handled carefully, monolayer homogeneity may be lost. Factors, such as the presence of multivalent ions in the aqueous phase and the pH of the subphase, can increase the monolayer stability prior to transfer. The relaxation time, which is the amount of time allowed for solvent evaporation before or after monolayer compression, can also affect the monolayer stability. After compression, the monolayer is typically not entirely stable but stabilizes over time. The decrease in SP when the area is held constant or the decrease in film area when the SP is held constant can be used to measure the monolayer stability. (40)

2 Aim of Study

This study was conducted to characterize the properties of simple lipid model of the SC barrier at the air-water interface. For such purpose, a lipid model of the SC composed by different Ceramides mixed with FFA (16-24) and Chol was used. Under physiological conditions, the interface between corneocytes and intercellular lipids is formed by the CLE. Under pathophysiological conditions, the formation of CLE is impaired or blocked. This allows the intercellular lipids to face a hydrophilic environment.

Furthermore, the influence of C24 Cer[NS] (Cer) replacement by C24 Cer[AP] (PhytoCer) or the lipid model behaviour was examined. Using the LB technique, lipid monolayers were formed and their SP-MMA isotherms were measured in order to investigate their behaviour.

Atomic force microscopy (AFM) was used to examine how the structure of the lipid monolayers changed with respect to the composition of the monolayers after they were transferred to a substrate. The supported monolayers could serve as a base for multi-layered models.

3 Materials and Methods

3.1 Materials

3.1.1 General Materials

- OHAUS Discovery Analytical Balance was bought from OHAUS Europe GmbH, Switzerland.
- pH Meter was purchased from METTLER TOLEDO.
- Hamilton Syringe was bought from Hamilton Bonaduz AG, Switzerland.
- Digital Dry Bath was bought from Labicom.
- Volumetric Flasks (2 mL, 1000 mL) were purchased from Avantor.
- Desiccator.
- Beakers (100 mL, 250 mL).
- Glass Pipette.
- Filtration Equipment with Nylon filter 0.45 μm.

3.1.2 Langmuir-Blodgett Instrument

For experiments with LB monolayers, the LB instrument (KSV NIMA, Biolin Scientific, Gothenburg, Sweden) was used. It consists of a frame, a set of barriers, a Langmuir trough and a balance with Wilhelmy plate (Figure 7).

The frame is the module that supports the LB trough and other parts of the instrument. The LB instrument is controlled by a computer through the KSV NIMA Interface Unit. The size of LB frame determines the maximal size of the trough that fits the instrument. A used standard frame is suitable for small to medium trough, for low to medium subphase volumes and for coating small to medium size samples.

The barriers are used to compress the monolayer and are placed on a barrier drive that is controlled by software. Delrin barriers, which are hydrophilic to avoid leakage under the barrier during compression, were used in the experiments.

The trough is a shallow chamber designed to hold a liquid phase. Troughs are hydrophobic as they are made of Poly(tetrafluoroethylene) (PTFE). Variety of trough sizes and specifications are available.

Some of them are adjusted for LB deposition and have a dipping well in its centre. When conducting vertical deposition, the well is required because the sample must pass through the film and below the liquid surface.

The SP is determined by an extremely sensitive balance measuring the force exerted on a Wilhelmy plate which is suspended across the air-liquid interface. The measuring range of the SP sensor is 0 to 300 mN/m with a resolution of 0.03 μN/m.

A dipping mechanism is a necessary piece of equipment for the regulated LB deposition on the samples.

A Platinum (Pt) Wilhelmy plate is used to measure the SP and it can be cleaned and reused multiple times.

The KSV NIMA Interface Unit allows an easy control of the trough barriers and dipping mechanism, all while standing right next to the instrument.

To provide greater environmental and sample control, all of these devices are enclosed in a cabinet made of an aluminium frame with clear acrylic glass panels on all sides, including the front doors.

A running PC program, KSV NIMA LB, is required to the interface unit to operate properly. The Manual Control option is available from the LB program main menu and is used to control the attached devices, such as barriers, balance and dipper. The Experimental Setup must be completed before each experiment in order to record the basic information about the experiment. The required details comprises the name and perimeter of the probe for balance, the name, width and area of the trough, the type of the subphase, and finally, the name, concentration, molecular weight and volume of the studied substance. The sample is applied as organic solution on the subphase surface. The volume of the sample depends on the concentration of the sample and on the mean area per lipid molecule required at the beginning of the experiment. The software also saves and analyses the gathered data.

A Bath/ Circulator (Julabo CD200F) is also connected to the instrument for temperature regulation, and it is controlled and operated independently from the LB software. The temperature working range is from -20 to +150°C, while the temperature stability is 0.03°C. (44) (45)

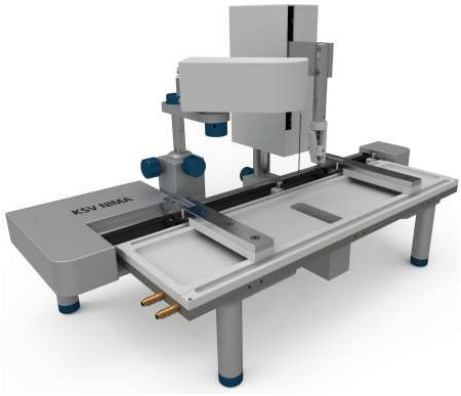

Figure 7: Langmuir-Blodgett Instrument. Adapted from (44). LB Instrument composed of the trough where the subphase is placed, the Langmuir film balance where the Wilhelmy plate is set to measure the Surface Pressure and the barriers for reducing the available surface area.

3.1.3 Langmuir-Blodgett Intrument Accessories

- LB troughs.
- LB balance calibration weight.
- Water levelling tool.
- Set of tools.
- Large platinum plate.
- Tweezers, stainless steel.
- Spatel/spoon, stainless steel.
- Glass beaker.
- 50 µl syringe. This syringe is used for spreading the monolayer material.
- MICA slides (15x15 mm^2) for deposition experiments (SPI Supplies, West Chester, Pennsylvania, USA).
- A soft paintbrush for cleaning the trough.
- An aspirator suction pump used for cleaning the subphase surface.
- Poly(tetrafluoroethylene) (PTFE) nozzle for the aspirator.
- Rubber hose, 1 x 3m.
- Package of 100 disposable nitrile protective gloves.
- Package of dust free paper tissues.
- Water tubing quick connectors.

3.1.4 Chemicals

Table 1: Chemicals used during the experiment

Chemical	Abbreviation	Molecular Structure	Supplier
Behenic Acid	$C_{22}H_{44}O_2$	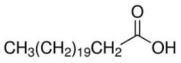	Sigma-Aldrich
Ultra Pure Water	H_2O	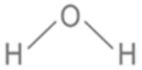	Milli-Q Water Purification System (MilliporeSigma)
Methanol	CH_4O	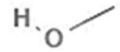	Penta Chemicals Unlimited
Chloroform	$CHCl_3$	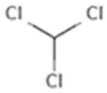	Penta Chemicals Unlimited
Acetic Acid	$C_2H_4O_2$	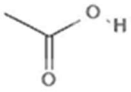	Penta Chemicals Unlimited
Sodium Acetate	$C_2H_3NaO_2$	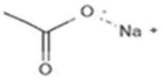	Lachema, Brno, Czech Republic
Cholesterol	$C_{27}H_{46}O$	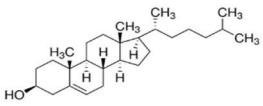	SIGMA
Fatty Acids Mixture of 16-24 carbons (FFA)			
1.8% Hexadecanoic acid	$CH_3(CH_2)_{14}COOH$	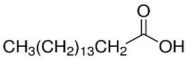	SIGMA
4.0% Octadecanoic acid	$CH_3(CH_2)_{16}COOH$	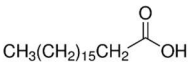	
7.6% Eicosanoic acid	$CH_3(CH_2)_{18}COOH$	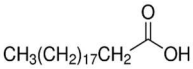	
47.8% Docosanoic acid/ Behenic Acid	$CH_3(CH_2)_{20}COOH$	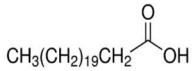	
38.8% Tetracosanoic acid/ Lignoceric Acid	$CH_3(CH_2)_{21}CH_2{}^{13}CO_2H$	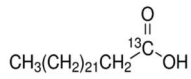	
α-hydroxy-N-lignoceroylphytosphingosine (PhytoCer)	$C_{42}H_{85}NO_5$	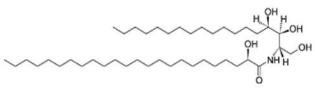	Synthesized at Department
N-lignoceroyl-D-erythro-sphingosine (Cer)	$C_{42}H_{83}NO_3$		Avanti Polar Lipids

3.2 Methods

3.2.1 Samples Preparation

3.2.1.1 Behenic Acid Sample

The isotherms of Behenic Acid were measured with the aim of find out a reproducible method of operating with a LB Instrument and obtaining reliable results.

Therefore, 1.51 mg of Behenic Acid was diluted in 1 mL of Chloroform-Methanol mixture at the ratio of 3:1 (V/V).

3.2.1.2 Lipid Samples modeling the SLB

FFA (16-24) were mixed in a molar ratio which is close to the native composition of human skin: 1.8% Hexadecanoic acid, 4.0% Octadecanoic acid, 7.6% Eicosanoic acid, 47.8% Docosanoic acid and 38.8% LIG. (5) The SC-modeling lipids were mixed at the constant 1:1:1 molar ratio of Ceramides/ FFA/ Chol. Cer contains a non hydroxylated fatty acid amid linked to SO base, while PhytoCer contains an alpha-hydroxylated fatty acid amid-linked to the PhytoSO base. Chol is a molecule with a steroid skeleton, a polar hydroxyl group and a short branched aliphatic chain. Fatty acids are amphiphilic molecules with a polar carboxyl group and a long saturated polymethylene chain of various length 16, 18, 20, 22 and 24 carbons.

Lipids were dissolved individually in 2:1 Chloroform/Methanol (V/V) and aliquots of lipid solutions were mixed according to the Table 2. The samples were dried under a stream of gaseous Nitrogen (N_2) at 37ºC using a Digital Dry Bath. The traces of solvents were removed in an vacuum desiccator. Each sample contained 1 mg of the dry lipid mixture and the molar ratios of individual components are in Table 3. The dry samples were stored in a freezer at -20ºC**.** Before being used, the dry lipid mixtures were redissolved in Chloroform:Methanol 2:1 (V/V) at 1 mg/mL.

Table 2: Aliquots of lipid solutions in lipid mixtures

Sample	Volume PhytoCer (µL)	Volume Cer (µL)	Volume Chol (µL)	Volume FFA (µL)
Cer/FFA/Chol (1:1:1)	0	338	151	161

PhytoCer/FFA/Chol (1:1:1)	309	0	147	157
Cer/PhytoCer/FFA/Chol (0.625:0.375:1:1)	118	210	149	160
PhytoCer/Cer/FFA/Chol (0.750:0.250:1:1)	233	83	148	158

Table 3: Molar ratios of lipid mixture components

Sample	PhytoCer (%)	Cer (%)	Chol (%)	FFA (%)
Cer/FFA/Chol (1:1:1)	0	1	1	1
PhytoCer/FFA/Chol (1:1:1)	1	0	1	1
Cer/PhytoCer/FFA/Chol (0.625:0.375:1:1)	0.375	0.625	1	1
PhytoCer/Cer/FFA/Chol (0.750:0.250:1:1)	0.750	0.250	1	1

3.2.2 Preparation of Acetate Buffer, pH 5.5

The amounts of each compound were calculated to prepare a solution at pH 5.5 that approximately corresponds to pH of the native human SC (39).

1.14296g of Sodium Acetate and 8 µL of Acetic Acid (99%) were used to prepare a buffer at pH=5.5. The compounds were dissolved in Milli-Q Water up to 1 L. Finally, the solution was filtered through 47 mm Nylon filters and the pH confirmed using a pH meter which revealed a value of pH 5.52.

3.2.3 Surface Pressure-Area Isotherms

To compare their area per molecule and compressibility, lipid monolayers, at an air–liquid interface, were studied using a medium LB trough with the width of 75 mm. The

area of the trough was calculated by measuring the length between the inner margins of barriers with a ruler and yielding a value of 15300 mm^2.

After filling the trough with the subphase a couple of mm above the edges, the temperature sensor, the barriers and the Wilhelmy plate were placed. The Wilhelmy plate was placed perpendicular to the barriers, in the center of the through. The purity of the water was then checked by setting the balance to zero at the maximum extension of the barriers and gradually bringing them closer together. It was considered clean when the SP was below 0.3 mN/m. If the SP raised significantly, this indicated the presence of surface-active impurities, as water does not change SP when compressed. In this case, contaminants were removed from the water surface using an aspirator.

The temperature of the subphase was stabilized at 22 °C before the experiment. The sample was applied by spreading it, drop by drop, at the cleaned air–liquid interface using a Hamilton Syringe. Solvent was let to evaporate in the period of 20 minutes. (8) Afterwards, the lipid film was compressed at the rate of 10 mm/min at 22ºC and the SP (π) recorded using a Platinum Wilhelmy plate. Resulting isotherms were expressed as a dependence of π [mN/m] on the mean area per a molecule (MMA) [$Å^2$]. Each experiment was repeated at least in triplicate. The mean molecular areas per lipid (Å) were calculated at 20 mN/m**.** The surface compression modulus ($1/C_S$), which represents a measure of stiffness, was calculated according to the Equation 3**,** where MMA is the mean area per a molecule**.** (11)

$$\mathbf{1/Cs = -MMA(\partial\pi/\partial MMA)} \qquad \mathbf{(3)}$$

3.2.3.1 Instrument Cleaning

At the end of each experiment, the instrument was cleaned. The barriers were taken down and washed in a fume hood, with Milli-Q water first and then with Methanol. The trough was emptied with an aspirator, removed from the frame and cleaned in a fume hood with commercial detergent and a soft brush. The detergent was first washed away with tap water, then rinsed with Milli-Q water and Chloroform: Methanol (3:1). Finally, the Wilhelmy plate and the temperature sensor were both rinsed with Chloroform: Methanol (3:1). All these equipment components were kept in a dust-free environment.

3.2.3.2 Behenic Acid Isotherm

Milli-Q water was used as a subphase. The applied amount of the Behenic Acid solution (1.51 mg/mL, MW=340.6 g/ mol) was 18 µL. This corresponded to the MMA of 41.9 Å at the beginning of the experiment. The experiment was performed according to the general protocol (Section 3.2.3).

3.2.3.3 Isotherms of SLB model

Acetate buffer (10 mM, pH 5,52) was used as a subphase. The applied amount of each lipid samples was 22 µL. The corresponded area per molecule at the beginning of the experiment is represented in Table 4. The experiment was performed according to the general protocol (Section 3.2.3).

Table 4: Average molecular Weight (MW) and mean area per molecule (MMA) at the beginning of the experiment

Sample	MW [g/ mol]	MMA [Å^2]
Cer/FFA/Chol (1:1:1)	460.08	53.20
PhytoCer/FFA/Chol (1:1:1)	472.12	54.50
Cer/PhytoCer/FFA/Chol (0.625:0.375:1:1)	465.03	53.70
PhytoCer/Cer/FFA/Chol (0.750:0.250:1:1)	469.28	54.20

3.2.4 Dipping Experiment

The Langmuir film balance can be used to build up highly aligned monolayers or multilayers of an amphiphile in addition to being used as a tool for monolayer studies. The controlled LB vertical deposition of the samples requires the use of a dipping mechanism. The goal of this experiment was to prepare a monolayer and to investigate it using AFM. Uniform monolayers can further serve as substrate to deposit multiple layers of defined composition in defined manner.

The transfer ratio (TR) value, which is defined as the area that the barriers have moved inwards (to maintain the SP) divided by the area of substrate that has been brought

through the monolayer, is a good indicator of the quality of the monolayer transfer on a substrate. The deposition will be better if the ratio is close to one. If the ratio is less than one some areas of the substrate were not deposited on and if it is greater than one, the film was either unstable or a multilayer was deposited.

A dipping experiment began similarly to an isotherm experiment. The trough was filled with Acetate buffer, pH= 5.5, the barriers and the temperature sensor were installed and the hydrophilic substrate, Mica (15 x 15 mm^2 ; SPI Supplies, West Chester, Pennsylvania, USA) was attached to the dipper sample holder such that it was parallel with the barriers. The quality of a deposition is affected by the orientation of a substrate in a dipping experiment, and a parallel orientation produces the best layers.

The substrate used in the experiment is hydrophilic. In this case, it must be immersed in the subphase at the start of the deposition to guarantee that the monolayer is properly oriented onto the substrate. The dipper was slowly lowered, using the Manual Control, and the motion was stopped just above the subphase surface. The dipper´s position was zeroed, and then the dipper was lowered until the coating part was completely immersed (position at -4,62 mm).

Afterwards, the sample was applied and the solvent was allowed to evaporate for 20 minutes. During this time, the relevant fields in the Experimental Setup, such as balance probe, trough area (8850 mm^2), substance properties and substrate dimensions (15x15 mm^2), were filled in.

The monolayer should be compressed enough to form a regular layer on the substrate, but not so tightly that it collapses when the substrate first comes into contact with the surface. The goal of deposition experiments is to raise the SP to a specific level and keep it at this value as the deposition progresses. The lipid monolayer at the air–liquid interface was compressed to 30 mN/m (target SP). At this point, the Dipper Controls window opened automatically and was filled with the required information (Table 5). In addition, the graph axes change to SP and barrier position against time.

After a 20 minutes waiting period to allow the monolayer to stabilize, the lipid monolayer at the air–liquid interface was transferred to a freshly cleaved mica that was raised vertically through the lipid film/ air–water interface at 0.5 mm/min. (3)

The monolayer was deposited onto the slide as the mica was lifted, and the amount of amphiphiles on the surface decreased. As a result, the SP decreased and the barriers

moved closer towards each other in order to compensate the decreasing SP. The software control windows close once the layer has been deposited. The scheme of the LB deposition process is presented in the Figure 8.

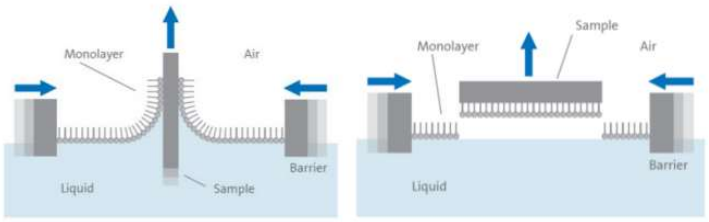

Figure 8: Deposition of a floating monolayer onto a hydrophilic solid substrate. Adapted from (43).

The cleaning process was performed according to the general protocol (Section 3.2.3.1).

The dipping experiment was performed on both Cer/FFA/Chol and PhytoCer/FFA/Chol mixtures and the procedure was repeated at least twice for each sample.

The supported monolayers were enclosed in glass flasks. To prevent oxidation, nitrogen gas was added to each sample before the analysis. The surface morphology of the samples was examined by the AFM technique at the Center of Materials and Nanotechnology, Faculty of Chemical Technology, University of Pardubice, nám. Čs. legií 565, 530 02 Pardubice, Czech Republic using an NTEGRA device ((NT-MDT, Hoenderparkweg 96 b, 7335 GX Apeldoorn, The Netherlands) in tapping mode with an HA_HR Etalon probe (NT-MDT, Hoenderparkweg 96 b, 7335 GX Apeldoorn, The Netherlands) in semi-contact mode. The topographical scans and height profiles were determined using appropriate software provided by the instrument manufacturer. (46)

Table 5: Dipper Controls

Upper Limit	5 mm
Speed Up	0.5 mm/min
Lower Limit	-4,62 mm
Speed Down	mm/min
Wait time	0,0 s
Number of Layers	1
Ignore First	0 mm

Averaging	0 mm

4 Results

4.1 Surface Pressure – Area Isotherms

4.1.1 Behenic Acid Isotherms

The representative pressure-area isotherms of the Behenic Acid are presented in Figure 9A. The lineshape can be splited into distinctive regions corresponding to the different molecular interaction forces occurring between the molecules in the floating film and the film and the subphase. Individual regions can be approximated with linear functions and the transitions between them can be recognised as a change of the slope (a kink in the isotherms).

While the MMA is above 30 $Å^2$ / molecule, the molecules do not significantly interact. This phase is known as the gaseous state (Figure 9B-G) due to the fact that molecules exert only small forces on one another and the resulting monolayer can be regarded as two-dimensional gas because of the large distances between the molecules. As intermolecular distances decrease, the molecules become close, begin to interact and SP begins to rise. This is presented here at MMA of about 18-30 $Å^2$ /molecule. This phase is referred to as the liquid state (Figure 9B-L1). At a MMA of less than 18 $Å^2$ /molecule, the molecules are very closely packed, molecular area is progressively reduced and form a rigid layer – solid state (Figure 9B-S). From a MMA area of about 17 $Å^2$ /molecule, molecules collapse due to the mechanical instability at very high SP and molecules are forced out of the interfacial film. Extrapolating a linear line through the measurement points in solid state to a SP of 0 mN/m gives the MMA for Behenic Acid in a water subphase, which should be 18-19 $Å^2$ /molecule. (47) The maximum compression modulus, which was calculated according to Equation 3, was 315 ± 110 mN/m.

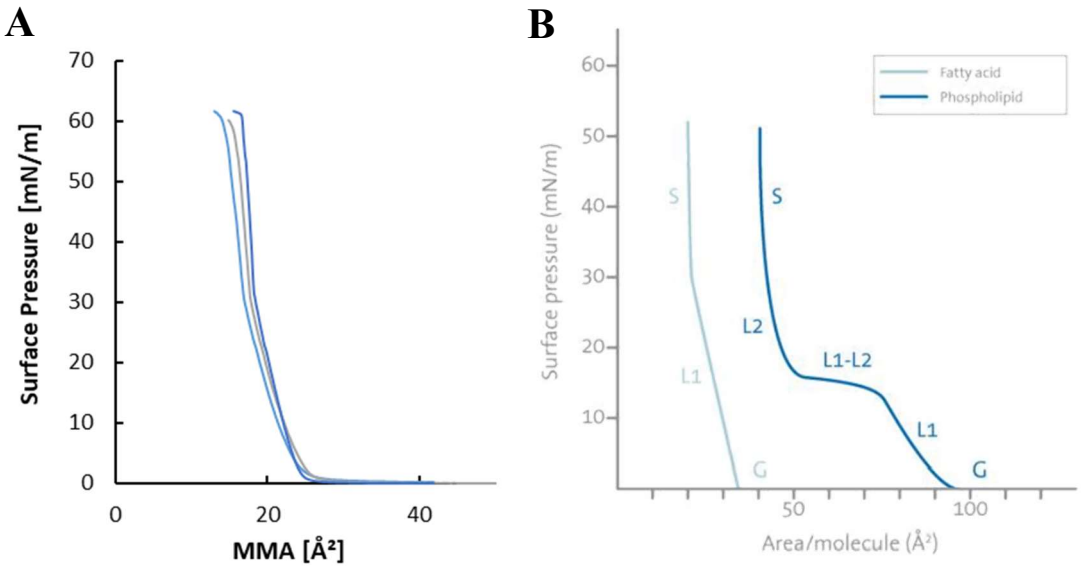

Figure 9: Pressure–area isotherms of Behenic Acid. Adapted from (44). (A) Three independent π-A isotherms were measured for Behenic Acid. The area is expressed as the mean molecular area (MMA) (B) Typical isotherm of a fatty acid and a phospholipid, showing the different types of transitions possible to detect using this technique. Monolayers generally exist in the gaseous state (G) and can change phases upon compression to become liquid-expanded layers (L1). Further compression results in a transition from L1 to the liquid-condensed phase (L2), and at even higher densities the monolayer finally enters the solid phase (S).

4.1.2 Isotherms of the SLB model

To compare the areas per lipid in ternary SLB model membranes containing equimolar amounts of FFA/ Chol and Ceramide or Phytoceramide, the SP versus MMA isotherms were recorded. (Figure 10A) The isotherms evidenced that the Cer/FFA/Chol sample exhibits less measurement variability than the samples which contain PhytoCer. Although the standard deviation (SD) for the measurements with sample PhytoCer/FFA/Chol was extremely high, we decided to use the average of the results (Figure 10B) as a reference as a strategy to compare the characteristics of each monolayer, always keeping in mind that it is just an approximation. For the Cer-containing sample, the collapse and the change from the gaseous state to the liquid-expanded phase both happened at a higher MMA than for the sample with PhytoCer.

Using this skin lipids models, we were able to observe a transition from the gaseous to the condensed state as well as the collapse of monolayers at lower MMA, evidenced by the low slope and the rounded shape. The PhytoCer-based model revealed a section in its shape between the condensed state and the collapse that resembles a phase transition.

This is a consequence of the high variability of the results obtained with this model as is apparent from large error bars. For better comparison between the different SLB model membranes, quantitative analysis of the isotherms can be performed. To estimate the approximate value of the solid-liquid phase transition, two linear sections of the pressure-area isotherm of each sample were selected and the intersection point that corresponds to the phase transition was determined. To determine the value of the SP [mN/m] where the collapse occurred in each sample, the part of the curve where the SP stabilised, which can be correlated with the monolayer collapse, was selected.

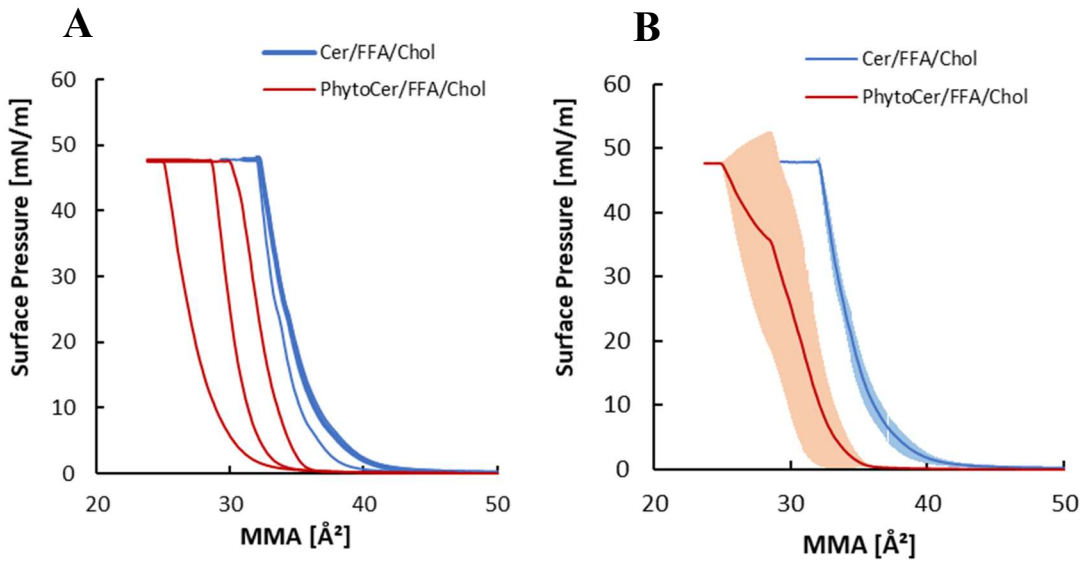

Figure 10: Pressure–area isotherms of ternary SLB models. (A) π-A isotherms were obtained in triplicate of ternary SLB models composed of 1:1:1 Cer/FFA/Chol (blue) or PhytoCer/FFA/Chol (red) mixtures. (B) Average of the π-area isotherms determined for the two mixtures. Error bars indicate SD of each experimental point.

The parameters obtained for the isotherms of these mixtures are summarized in Table 6. The mixture Cer/FFA/Chol showed larger MMA at the same SP than the analogous mixture with PhytoCer. As shown in the table, at 30 mN/m, the MMA was slightly higher for Cer/FFA/ Chol (33.4 ± 0.4 $Å^2$) compared to PhytoCer/FFA/Chol (29.3 ± 2.6 $Å^2$). For Cer/FFA/Chol, the isotherm shape revealed a gaseous−liquid transition at about 0.8 mN/m and 36.1 $Å^2$ and the collapse was detected at 47.8 ± 0.1 mN/m and 31.3 ± 0.01 $Å^2$. In contrast, for PhytoCer/FFA/Chol, the isotherm shape revealed a gaseous−liquid transition at 0.2 mN/m and 33.6 $Å^2$ and the collapse occurred at higher SP (47.7 ± 0.2 mN/m) and lower MMA (26.9 ± 2.7 $Å^2$) compared to the other ternary

mixture. This refers to more effective packing of molecules of the PhytoCer-based mixture relative to the Cer-based mixture. The maximum compression modulus was also different for these mixtures and higher for Cer (498 ± 108 mN/m) compared to PhytoCer (455 ± 84 mN/m), showing that it has larger stiffness and is more resistant to compression.

Table 6: Mean Molecular Areas (MMA), Surface Pressure (SP, π) at which collapse occurs and maximum compression modulus (1/Cs) determined from the surface-pressure isotherms measured for the different SLB model mixtures. The ratio between Cer and PhytoCer in the mixtures is also shown in the table. The values correspond to the average ± SD of 3 independent experiments.

Sample	PhytoCer:Cer [mol/ mol]	MMA [Å^2] π = 20 [mN/m]	MMA [Å^2] π = 30 [mN/m]	$\pi_{collapse}$ [mN/m]	1/Cs [mN/m]
Cer/FFA/Chol (1:1:1)	0 : 1	34.4 ± 0.2	33.4 ± 0.4	47.8 ± 0.1	498 ± 108
PhytoCer/FFA/Chol (1:1:1)	1 : 0	30.7 ± 2,5	29.3 ± 2.6	47.7 ± 0.2	455 ± 84
Cer/PhytoCer/FFA/Chol (0.625:0.375:1:1)	0.375 : 0.625	33.8 ± 3.0	31.8 ± 3.2	49.8 ± 0.2	441± 41
PhytoCer/Cer/FFA/Chol (0.750:0.250:1:1)	0.750 : 0.250	33.0 ± 2.7	31.4 ± 2.5	48.1 ± 0.2	311± 18

The procedure was repeated using the samples Cer/PhytoCer/FFA/Chol and PhytoCer/Cer/FFA/Chol. Figure 11A depicts representative π-A isotherms. Like the ternary SLB model containing PhytoCer, a strong variability was observed in the π-A isotherms of quaternary SLB models and therefore the results reflect a high level of uncertainty (Figure 11B). As shown in Table 6, at a SP of 30 mN/m, the MMA of Cer (Cer/PhytoCer/FFA/Chol (0.625:0.375:1:1) (31.8 ± 3.2 Å^2) and PhytoCer Cer/PhytoCer/FFA/Chol (0.25:0.75:1:1) (31.4 ± 2.5 Å^2) did not significantly differ within the experimental errors. The isotherm shape revealed a gaseous−liquid transition for sample Cer/PhytoCer/FFA/Chol at about 0.2 mN/m and 37.6 Å^2 and the collapse was detected at 49.8 ± 0.2 mN/m and 30.0 ± 3.0 Å^2. In contrast, for

PhytoCer/Cer/FFA/Chol, the isotherm shape revealed a gaseous-liquid transition at 0.2 mN/m and 36.6 Å^2 and the collapse was detected at 48.1 ± 0.2 mN/m and 27.4±2.4 Å^2.

Across the entire range of SP's, similar differences were observed. The isotherm of the sample Cer/PhytoCer/FFA/Chol is slightly shifted to the right hand side when compared to the sample which contains a higher amount of PhytoCer, which is consistent with the outcomes found using the samples Cer/FFA/Chol and PhytoCer/FFA/Chol. The isotherm indicated that the sample with Cer/PhytoCer/FFA/Chol was more rigid (the maximum compression modulus was 441 ± 41 mN/m) than that with the PhytoCer/Cer/FFA/Chol (the maximum compression modulus was 311 ± 18 mN/m).

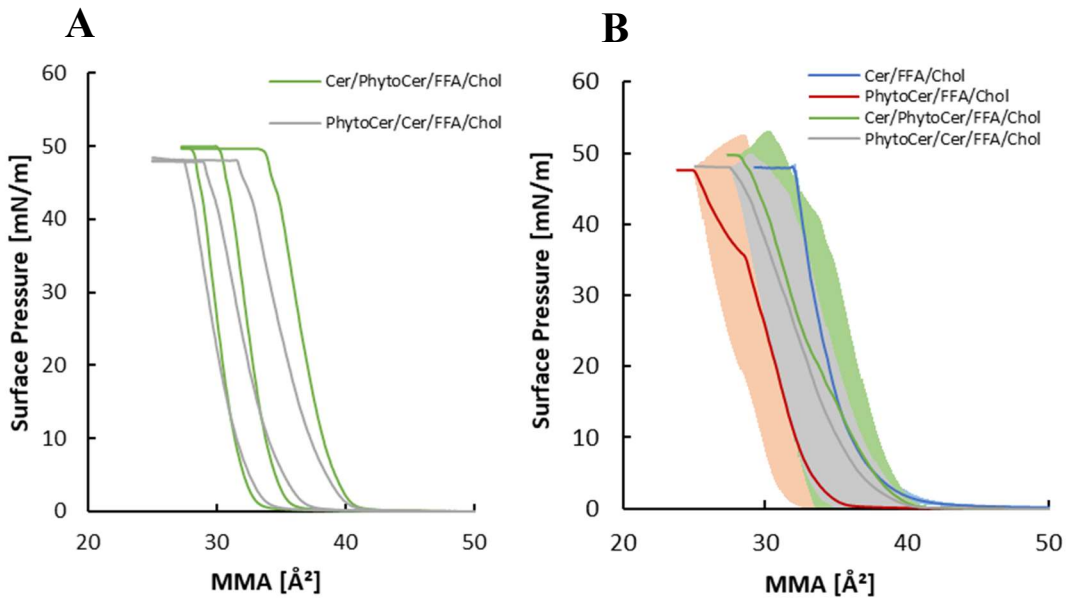

Figure 11: Pressure–area isotherms of quaternary SLB models. (A) π-A isotherms were obtained in triplicate of quaternary SLB models composed of 0.625:075:1:1 Cer/PhytoCer/FFA/Chol (green) or 0.25:0.75:1:1 Cer/PhytoCer/FFA/Chol (grey) mixtures. (B) Average of the π-area isotherms determined for the four mixtures. Error bars indicate SD of each experimental point.

4.2 Dipping Experiment

Monolayers at an air/water interface were then transferred to a mica support at 30 mN/m and studied using AFM to visualize the different lipid domains. The experiment was repeated, at least twice, for samples Cer/FFA/Chol and PhytoCer/FFA/Chol. Figure 12A shows that two distinct domains are visible in the AFM images of Cer/FFA/Chol

(1:1:1) monolayer. A large fraction of the surface is covered with higher domains, which appear in the AFM image as lighter coloured areas. This phase formed circular irregularly organized and interconnected domains. A lower, darker-coloured phase covers the remaining surface. The height difference between the two phases is 0.9 ± 0.2 nm. There were also some white spots on the surface, indicating the presence of impurities. We suppose that the samples were contaminated during the manipulation or transport. Figure 12B shows AFM images of a transferred mixed monolayer prepared at an equimolar ratio of PhytoCer/FFA/Chol. Four different phases were observed in this film: i) darker areas corresponding to domains with lower height; ii) small circular domains seen as bright spots of higher height; iii) many irregular and interconnected structures with intermediate height and iv) fibre-like structures with a thickness of individual fibrillar structures around 20 nm. The height difference between circular and the irregular domains were 0.8 ± 0.1 nm.

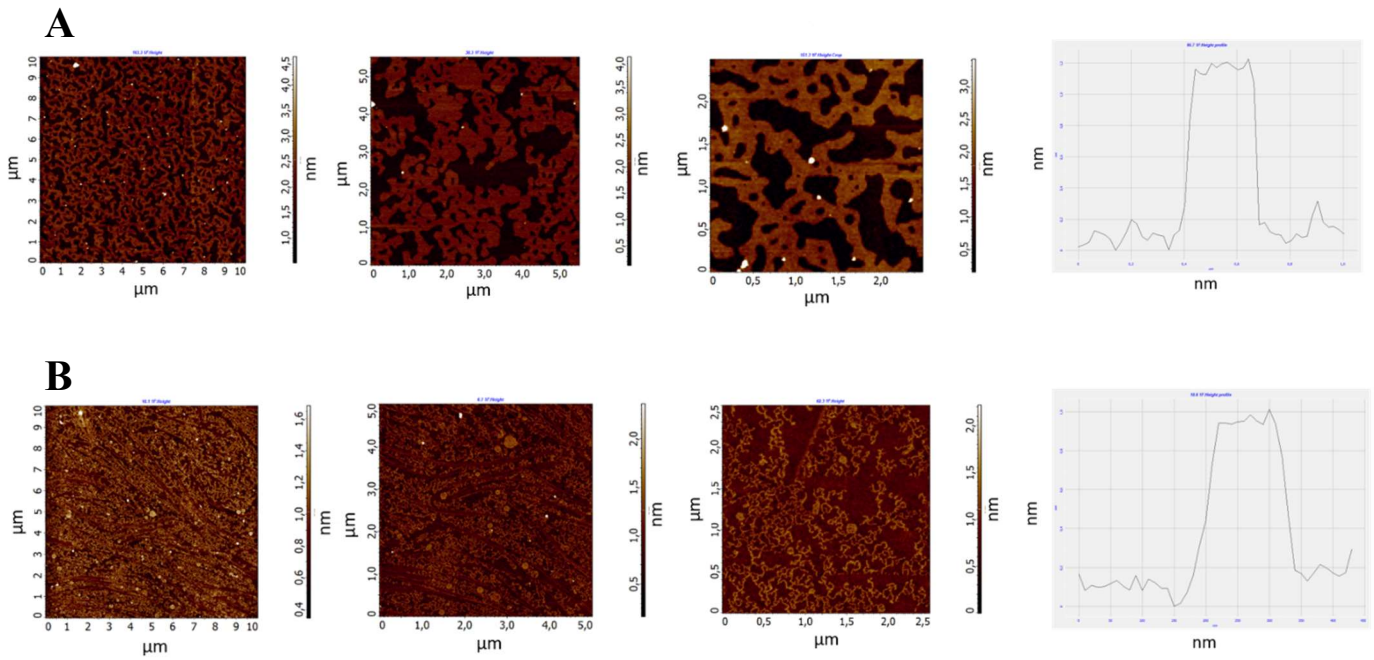

Figure 12: AFM images and a height profile of ternary SLB models. AFM images and height profile were obtained in duplicate of ternary SLB models composed of (A) 1:1:1 Cer/FFA/Chol or (B) PhytoCer/FFA/Chol.

5 Discussion

These techniques were employed with the aim to reveal the behaviour of the skin lipids models, specifically in terms of area per molecule and compressibility. The behaviour of lipids in the monolayer is relevant for the structural requirements and mechanisms of action of Cer and PhytoCer in the lipidic layers of the skin, which are still uncertain, limiting the design of skin barrier repair agents or wider use of transdermal drug delivery. (3) The proper barrier function of the skin is guaranteed in healthy epidermis by a monolayer of ω -hydroxyceramides covalently attached to the outer surface of the cornified envelope - the CLE. (14) The proper formation of the cornified envelope and the intercellular lipid lamellae depend on the CLE. In the presence of autosomal recessive congenital ichthyosis (ARCI) and an ALOX12$^{-/-}$ mouse model, the CLE is impaired or lacking, the intercellular lipid lamellae is poorly organized, and the cornified envelope is thin, compromising the homeostasis of SLB. (48)

Cer, PhytoCer, FFA, and Chol were used to create a lipid membrane model. Model skin lipid membranes have been widely used to investigate the relationships between lipid structure and composition, lipid organization, and membrane permeability. (3) This membrane model does not include ω-O-acyl-Ceramides, Corneocytes or CholS which are important components of the skin barrier. As a result, the lipid composition is more straightforward. However, previous studies discovered a relationship between the permeability of this straightforward membrane model and the structure of ceramide molecules. (49) The advantage of such a simplified model is that we can easily control and vary its composition and determine biophysical parameters which are necessary when studying specific properties of ceramides and to provide structure-activity relationships.

In contrast to what was recorded in Behenic Acid samples, the phase transition between the liquid and solid states could not be identified with the skin lipids models. Only the condensed and the transition to the monolayer collapse could be distinguished, as evidenced by the different slopes of the different parts of the isotherm curve. This is in line with the findings of previous studies on both C24 Cer and C16 Cer-based monolayers. (8) (3) The MMA of 40.1 ± 1.5 Å^2 at the lift-off (π = 1.5 mN/m) determined herein for Cer/FFA/Chol, is in the same range as previously reported for Cer, LIG, Chol and CholS composed SLB models (36 ± 2 Å^2), (8) suggesting that these

models present some similarities at low SP. Moreover, the maximum compression modulus for the mixture studied herein is comparable (498 ± 108 mN/m) relative to the value reported for Cer, LIG, Chol and CholS composed SLB models (508 mN/m). (8) At 20 mN/m, we obtained an MMA of 34.4 ± 0.2 $Å^2$ in the Cer/FFA/Chol sample. This result is in good agreement with a previous study on Cer/FFA/Chol/CholS monolayers that reported an area of 32.5 ± 1.5 $Å^2$ at the same SP. (3)

The results obtained on Langmuir monolayers showed a difference in the shape position of the π-A isotherms depending on the lipid composition of the SLB model used. The greater the amount of PhytoCer in each sample, the more the corresponding curve is positioned further to the left of the graph (at lower MMA), indicating the ability of the lipid chains of this model to pack more tightly. We found that collapse occurs, for all samples, at a similar SP and lower MMA value for the PhytoCer/FFA/Chol sample, with the highest MMA value of the collapse corresponding to the Cer/FFA/Chol sample, corroborating a more efficient packing in the models containing PhytoCer.

The obtained results suggest that PhytoCer-based model is more compressed at the same SP relative to Cer-based model, implying that the lipid molecules in the PhytoCer-containing mixture are more condensed than those in the Cer mixture. This happens because of the structural differences between these molecules, which affect their behaviour in membranes and permeability (6) due to significant differences in H-bonding interactions and water penetration propensity. (7)

The acyl chain length affects the structure and permeability of the skin's lipid barrier. Cer and PhytoCer both have very long acyl chains with 24 carbons that are essential for the formation of densely packed impermeable lipid lamellae. (3)

Cer contains a SO, which is unsaturated due to a trans double bond at position 4-5, and non-hydroxylated fatty acid. SO-containing ceramides subclasses account for up to a quarter of all free SC Ceramides. (16) The non-hydroxy acyl SO-type ceramides are critical for a healthy skin barrier. (3) The role of the double bond has been a point of contention, and it needs to be clarified. In comparison to ceramides, dihydroceramides (dCer), which lack the 4-5 trans double bond, have a distorted polar head region and less hydrogen bonding with water. It was also proved that saturation of the C4 trans double bond increased the thermal stability of the ordered phases, implying stronger

cohesive forces in dCer membranes. (49) It is also known that the dCer/Cer ratio is important for lipid barrier homeostasis. (50)

Phytoceramide is structurally characterized by a saturated sphingoid base with an additional hydroxyl group (PhytoSO) linked to a fatty acid chain containing an alpha-hydroxyl group, which confers a more hydrophilic character to this ceramide. Phytoceramides subclasses contribute up to 32 percent of free SC Ceramides and the non-hydroxy acyl phytoceramide based membranes showed higher permeability relative to the membranes based on SO- or dihydrosphingosine-derived ceamides. (16) In comparison to dihydroceramides or ceramides with the same chain lengths, phytoceramides with very long C24 acyl chains increased the permeability of the model lipid membranes. (16)

Summarizing, we did not observe significant differences between Cer and PhytoCer-based models in their behavior at the water-air interface. Isotherms had similar shapes, and there weren't several differences in the average area per molecule.

A high variability between isotherms of the same lipid composition was observed for SLB models containing PhytoCer (PhytoCer/FFA/Chol, Cer/PhytoCer/FFA/Chol and PhytoCer/Cer/FFA/Chol). These differences are unlikely to result from uncorrected experimental procedures, since reproducibility was obtained both for control samples containing Behenic Acid, and mixtures of Cer/FFA/Chol. These observations also suggest that differences in the isotherms were likely caused by the presence of PhytoCer in the mixture. The data should be interpreted cautiously because Phytocer was synthetized in house and one cannot exclude the possibility that it contained traces of impurities below the detection limit of common analytical methods.

The phase behaviour of the Cer and PhytoCer-based models was also investigated using AFM after the monolayers were transferred to Mica substrate. In both mixtures, the AFM topographical images of the supported monolayers revealed separated domains, indicating that the systems are not entirely miscible which led to lateral segregation. The shapes and sizes of these domains, on the other hand, changed between samples. AFM images of a transferred monolayer prepared with a Cer/FFA/Chol mixture showed a two-domain film with a height difference between the two phases of ≈1 nm, which is comparable to previous studies that report a height difference between these domains of 1.2 ± 0.2 nm. (8)

However, a much more complex behaviour was observed for ternary SLB models containing PhytoCer. In fact, four types of domains could be observed in the PhytoCer/FFA/ Chol mixture, including fibre-like structures. We hypothesized that PhytoCer fibre-like domains could be artefacts of mechanical origin. However, we estimated the thickness of the individual fibre-like structures to be around 20 nm. Therefore, their origin in mechanical damage is unlikely. The existence of so many different types of domains in these mixtures points towards a complex phase behaviour of this ceramide, which might justify the strong differences observed between π-A isotherms measured for the same mixture. Nonetheless, and despite the presence of different domains, including the fibres in the AFM images of two different experiments with PhytoCer-containing ternary SLB mixtures, more research is needed to determine whether it is a property of PhytoCer or originated by lipid impurities derived from in-house synthesis of this lipid.

The presence of numerous domains with various sizes and shapes, including tubular structures, in the Phyto/FFA/Chol sample might be the cause of the variability of the results found in monolayers and even for an increased complexity of their biophysical behaviour.

Thus, research on this topic will continue in order to identify the exact source of the problem and confirm the accuracy of the findings.

6 Conclusion

Our research focused on analysing the behaviour of lipid models containing Ceramide/FFA/Chol in a 1:1:1 equimolar ratio. We varied the composition of ceramides present in each sample to investigate how the different chemical structures affect the lipid behaviour in the SLB. LB instrument was used to create the lipid monolayers at the air/water interface and their SP as a function of the MMA (isotherms) were measured. A dipping experiment was carried out to transfer a monolayer onto a solid substrate (Mica). The monolayers were also analysed using AFM. The behaviour of the various models showed some differences in air/water interface. The condensation of the PhytoCer-based model was achieved at lower MMA, implying that PhytoCer-based model can be more effectively packed in a compacted monolayer structure. The PhytoCer packing is related to its chemical structure. The AFM results revealed the presence of two and four domains in Cer and PhytoCer-based model, respectively. Despite the remarkable studies and the recent technological developments in this field, the structure and properties of the SLB in the SC, as well as the role of the main lipid components in maintaining homeostasis, remain uncertain. Further studies can be developed using LB technique since it allows the construction of a highly organized films by sequentially dipping a solid substrate up and down through the monolayer. This enables the production of LB films with a larger number of layers and different lipids composition. Additionally, more complex models can be created. With the development of better laboratory techniques and data analyses, doubts concerning this field are gradually being resolved. This study could be extended using additional layers with a more complex composition, such as isolated skin lipids, resembling the human SC.

References

1. van Smeden J, Janssens M, Gooris GS, Bouwstra JA. The important role of stratum corneum lipids for the cutaneous barrier function. Biochim Biophys Acta. 2014 Mar;1841(3):295–313.
2. Holleran WM, Takagi Y, Uchida Y. Epidermal sphingolipids: Metabolism, function, and roles in skin disorders. FEBS Lett. 2006 Oct 9;580(23):5456–66.
3. Skolová B, Janůšová B, Zbytovská J, Gooris G, Bouwstra J, Slepička P, et al. Ceramides in the skin lipid membranes: length matters. Langmuir ACS J Surf Colloids. 2013 Dec 17;29(50):15624–33.
4. Janůšová B, Zbytovská J, Lorenc P, Vavrysová H, Palát K, Hrabálek A, et al. Effect of ceramide acyl chain length on skin permeability and thermotropic phase behavior of model stratum corneum lipid membranes. Biochim Biophys Acta BBA - Mol Cell Biol Lipids. 2011 Mar 1;1811(3):129–37.
5. Groen D, Gooris GS, Bouwstra JA. Model membranes prepared with ceramide EOS, cholesterol and free fatty acids form a unique lamellar phase. Langmuir ACS J Surf Colloids. 2010 Mar 16;26(6):4168–75.
6. Vávrová K, Kováčik A, Opálka L. Ceramides in the skin barrier. Acta Fac Pharm Univ Comen. 2017 Jan 27;64.
7. Mendelsohn R, Rerek ME, Moore DJ. Infrared spectroscopy and microscopic imaging of stratum corneum models and skin. Invited Lecture. Phys Chem Chem Phys. 2000 Jan 1;2(20):4651–7.
8. Pullmannová P, Pavlíková L, Kováčik A, Sochorová M, Školová B, Slepička P, et al. Permeability and microstructure of model stratum corneum lipid membranes containing ceramides with long (C16) and very long (C24) acyl chains. Biophys Chem. 2017 May;224:20–31.
9. Forslind B. A domain mosaic model of the skin barrier. Acta Derm Venereol. 1994;74(1):1–6.
10. Damien F, Boncheva M. The extent of orthorhombic lipid phases in the stratum corneum determines the barrier efficiency of human skin in vivo. J Invest Dermatol. 2010 Feb;130(2):611–4.
11. Nováčková A, Sagrafena I, Pullmannová P, Paraskevopoulos G, Dwivedi A, Mazumder A, et al. Acidic pH Is Required for the Multilamellar Assembly of Skin Barrier Lipids In Vitro. J Invest Dermatol. 2021 Aug;141(8).
12. ten Grotenhuis E, Demel RA, Ponec M, Boer DR, van Miltenburg JC, Bouwstra JA. Phase behavior of stratum corneum lipids in mixed Langmuir-Blodgett monolayers. Biophys J. 1996 Sep;71(3):1389–99.
13. Rabionet M, Gorgas K, Sandhoff R. Ceramide synthesis in the epidermis. Biochim Biophys Acta. 2014 Mar;1841(3):422–34.
14. Wertz PW. Lipid Metabolic Events Underlying the Formation of the Corneocyte Lipid Envelope. Skin Pharmacol Physiol. 2021;34(1):38–50.

15. Pinto SN, Silva LC, Futerman AH, Prieto M. Effect of ceramide structure on membrane biophysical properties: The role of acyl chain length and unsaturation. Biochim Biophys Acta BBA - Biomembr. 2011 Nov;1808(11):2753–60.

16. Školová B, Kováčik A, Tesař O, Opálka L, Vávrová K. Phytosphingosine, sphingosine and dihydrosphingosine ceramides in model skin lipid membranes: permeability and biophysics. Biochim Biophys Acta Biomembr. 2017 May;1859(5):824–34.

17. Stiban J, editor. Bioactive Ceramides in Health and Disease: Intertwined Roles of Enigmatic Lipids [Internet]. Cham: Springer International Publishing; 2019 [cited 2022 Aug 16]. (Advances in Experimental Medicine and Biology; vol. 1159).

18. Ventura AE, Varela ARP, Dingjan T, Santos TCB, Fedorov A, Futerman AH, et al. Lipid domain formation and membrane shaping by C24-ceramide. Biochim Biophys Acta BBA - Biomembr. 2020 Oct;1862(10):183400.

19. Školová B, Hudská K, Pullmannová P, Kováčik A, Palát K, Roh J, et al. Different Phase Behavior and Packing of Ceramides with Long (C16) and Very Long (C24) Acyls in Model Membranes: Infrared Spectroscopy Using Deuterated Lipids. J Phys Chem B. 2014 Sep 4;118(35):10460–70.

20. Castro BM, Prieto M, Silva LC. Ceramide: A simple sphingolipid with unique biophysical properties. Prog Lipid Res. 2014 Apr;54:53–67.

21. Carreira AC, Ventura AE, Varela ARP, Silva LC. Tackling the biophysical properties of sphingolipids to decipher their biological roles. Biol Chem. 2015 Jun 1;396(6–7):597–609.

22. Grouleff J, Irudayam SJ, Skeby KK, Schiøtt B. The influence of cholesterol on membrane protein structure, function, and dynamics studied by molecular dynamics simulations. Biochim Biophys Acta BBA - Biomembr. 2015 Sep;1848(9):1783–95.

23. Castro BM, Prieto M, Silva LC. Ceramide: A simple sphingolipid with unique biophysical properties. Prog Lipid Res. 2014 Apr;54:53–67.

24. Carreira AC, Santos TC, Lone MA, Zupančič E, Lloyd-Evans E, de Almeida RFM, et al. Mammalian sphingoid bases: Biophysical, physiological and pathological properties. Prog Lipid Res. 2019 Jul;75:100988.

25. Mishra SK, Stephenson DJ, Chalfant CE, Brown RE. Upregulation of human glycolipid transfer protein (GLTP) induces necroptosis in colon carcinoma cells. Biochim Biophys Acta BBA - Mol Cell Biol Lipids. 2019 Feb;1864(2):158–67.

26. Nagahashi M, Tsuchida J, Moro K, Hasegawa M, Tatsuda K, Woelfel IA, et al. High levels of sphingolipids in human breast cancer. J Surg Res. 2016 Aug;204(2):435–44.

27. Wojewodka G, De Sanctis JB, Radzioch D. Ceramide in Cystic Fibrosis: A Potential New Target for Therapeutic Intervention. J Lipids. 2011;2011:1–13.

28. Czubowicz K, Strosznajder R. Ceramide in the Molecular Mechanisms of Neuronal Cell Death. The Role of Sphingosine-1-Phosphate. Mol Neurobiol. 2014 Aug;50(1):26–37.

29. Mosbech M, Olsen ASB, Neess D, Ben-David O, Klitten LL, Larsen J, et al. Reduced ceramide synthase 2 activity causes progressive myoclonic epilepsy. Ann Clin Transl Neurol. 2014 Feb;1(2):88–98.

30. Aburasayn H, Al Batran R, Ussher JR. Targeting ceramide metabolism in obesity. Am J Physiol-Endocrinol Metab. 2016 Aug 1;311(2):E423–35.

31. Laaksonen R, Ekroos K, Sysi-Aho M, Hilvo M, Vihervaara T, Kauhanen D, et al. Plasma ceramides predict cardiovascular death in patients with stable coronary artery disease and acute coronary syndromes beyond LDL-cholesterol. Eur Heart J. 2016 Jul 1;37(25):1967–76.
32. Andrews NW, Almeida PE, Corrotte M. Damage control: cellular mechanisms of plasma membrane repair. Trends Cell Biol. 2014 Dec;24(12):734–42.
33. Siskind LJ, Kolesnick RN, Colombini M. Ceramide forms channels in mitochondrial outer membranes at physiologically relevant concentrations. Mitochondrion. 2006 Jun;6(3):118–25.
34. Carreira AC, Ventura AE, Varela ARP, Silva LC. Tackling the biophysical properties of sphingolipids to decipher their biological roles. Biol Chem. 2015 Jun 1;396(6–7):597–609.
35. Yu FPS, Amintas S, Levade T, Medin JA. Acid ceramidase deficiency: Farber disease and SMA-PME. Orphanet J Rare Dis. 2018 Dec;13(1):121.
36. Ehlert K, Frosch M, Fehse N, Zander A, Roth J, Vormoor J. Farber disease: clinical presentation, pathogenesis and a new approach to treatment. Pediatr Rheumatol. 2007 Dec;5(1):15.
37. Montero J, Morales A, Llacuna L, Lluis JM, Terrones O, Basañez G, et al. Mitochondrial Cholesterol Contributes to Chemotherapy Resistance in Hepatocellular Carcinoma. Cancer Res. 2008 Jul 1;68(13):5246–56.
38. Elustondo P, Martin LA, Karten B. Mitochondrial cholesterol import. Biochim Biophys Acta BBA - Mol Cell Biol Lipids. 2017 Jan;1862(1):90–101.
39. Ishikawa J, Narita H, Kondo N, Hotta M, Takagi Y, Masukawa Y, et al. Changes in the Ceramide Profile of Atopic Dermatitis Patients. J Invest Dermatol. 2010 Oct;130(10):2511–4.
40. Girard-Egrot AP, Blum LJ. Langmuir-Blodgett Technique for Synthesis of Biomimetic Lipid Membranes. In: Martin DK, editor. Nanobiotechnology of Biomimetic Membranes [Internet]. Boston, MA: Springer US; 2007 [cited 2022 Feb 3]. p. 23–74. (Fundamental Biomedical Technologies).
41. Mildner J, Wnętrzak A, Dynarowicz-Latka P. Cholesterol and Cardiolipin Importance in Local Anesthetics–Membrane Interactions: The Langmuir Monolayer Study. J Membr Biol. 2019 Feb;252(1):31–9.
42. Barnes G, Gentle I. Interfacial Science: An Introduction. Second Edition. Oxford, New York: Oxford University Press; 2011. 352 p.
43. Schwartz DK. Langmuir-Blodgett film structure. Surf Sci Rep. 1997 Jan;27(7–8):245–334.
44. KSV-NIMA-LB-Software-Manual_v1.4.pdf [Internet]. [cited 2022 Feb 3].
45. Scientific B. Langmuir and Langmuir-Blodgett Deposition Troughs Modules and Accessories. Biolin Scientific AB, Hängpilsgatan 7, SE-426 77 Västra Frölunda: Biolin Scientific; 2013
46. Jancalek J, Palka K, Kurka M, Slang S, Vlcek M. Comparison of solution processed As33S67 thin films deposited using primary amines of various aliphatic chain length. J Non-Cryst Solids. 2020 Dec;550:120382.

47. Morelis RM, Girard-Egrot AP, Coulet PR. Dependence of Langmuir-Blodgett film quality on fatty acid monolayer integrity. 1. Nucleation crystal growth avoidance in the monolayer through the optimized compression procedure. Langmuir. 1993 Nov;9(11):3101–6.

48. Crumrine D, Khnykin D, Krieg P, Man MQ, Celli A, Mauro TM, et al. Mutations in Recessive Congenital Ichthyoses Illuminate the Origin and Functions of the Corneocyte Lipid Envelope. J Invest Dermatol. 2019 Apr;139(4):760–8.

49. Skolová B, Jandovská K, Pullmannová P, Tesař O, Roh J, Hrabálek A, et al. The role of the trans double bond in skin barrier sphingolipids: permeability and infrared spectroscopic study of model ceramide and dihydroceramide membranes. Langmuir ACS J Surf Colloids. 2014 May 20;30(19):5527–35.

50. Takagi S, Tojo H, Tomita S, Sano S, Itami S, Hara M, et al. Alteration of the 4-sphingenine scaffolds of ceramides in keratinocyte-specific Arnt-deficient mice affects skin barrier function. J Clin Invest. 2003 Nov 1;112(9):1372–82.